AGU PUBLICATIONS

JGR

Journal of Geophysical Research: Atmospheres

RESEARCH ARTICLE
10.1002/2016JD026249

Key Point:
- The apparent polarizability of voids within porous aerosol is useful for predicting their extinction

Correspondence to:
C. Haspel,
caryn@vms.huji.ac.il

Citation:
Haspel, C., and G. Adler (2017), The concept of apparent polarizability for calculating the extinction of electromagnetic radiation by porous aerosol particles, *J. Geophys. Res. Atmos.*, *122*, 3944–3952, doi:10.1002/2016JD026249.

Received 16 NOV 2016
Accepted 16 MAR 2017
Accepted article online 22 MAR 2017
Published online 4 APR 2017

The concept of apparent polarizability for calculating the extinction of electromagnetic radiation by porous aerosol particles

C. Haspel[1] and G. Adler[2,3]

[1]Fredy and Nadine Herrmann Institute of Earth Sciences, The Hebrew University of Jerusalem, Jerusalem, Israel, [2]Chemical Sciences Division, NOAA Earth System Research Laboratory (ESRL), Boulder, Colorado, USA, [3]Cooperative Institute for Research in Environmental Sciences, University of Colorado, Boulder, Colorado, USA

Abstract In the current study, the electromagnetic properties of porous aerosol particles are calculated in two ways. In the first, a porous target input file is generated by carving out voids in an otherwise homogeneous particle, and the discrete dipole approximation (DDA) is used to compute the extinction efficiency of the particle assuming that the voids are near vacuum dielectrics and assuming random particle orientation. In the second, an effective medium approximation (EMA) style approach is employed in which an apparent polarizability of the voids is defined based on the well-known solution to the problem in classical electrostatics of a spherical cavity within a dielectric. It is found that for porous particles with smaller overall diameter with respect to the wavelength of incident radiation, describing the voids as near vacuum dielectrics within the DDA sufficiently reproduces measured values of extinction efficiency, whereas for porous particles with moderate to larger overall diameters with respect to the wavelength of the radiation, the apparent polarizability EMA approach better reproduces the measured values of extinction efficiency.

1. Introduction

Porous particles are fairly widespread in nature and in man-made technology. Examples of natural porous particles include interplanetary dust and interstellar particles [*Bohren and Huffman*, 1983; *Kolokolova and Gustafson*, 2001; *Wolff et al*., 1998], as well as terrestrial dust and volcanic ash (see, e.g., *Jeong and Nousiainen* [2014] and *Kylling et al*. [2014]). Examples of man-made porous particles include particles created during "freeze-drying," which is a technique commonly used in the pharmaceutical industry and food industry. This industrial freeze-drying process is known to alter particle size and morphology, creating larger particles and a "sponge-like" porous structure [*Zijlstra et al*., 2004]. A summary of the mechanisms by which pore formation is expected to occur in foods during freeze-drying can be found in *Rahman* [2001].

In two recent studies, we suggested that the structural changes that occur in industrial freeze-dried materials also take place in organic atmospheric aerosol particles within deep convective clouds [*Adler et al*., 2013; *Adler et al*., 2014]. As part of this process, once the aerosol particle is formed/emitted and as it ascends within a rising air parcel, the aerosol particle adsorbs water and undergoes hygroscopic growth to form an organic aerosol-water droplet. As the air particle continues to ascend to higher altitudes, the droplets containing the organic solute freeze. Following the growth and ice formation, the air parcel encounters subsaturated conditions, and the ice sublimates. The unique porous morphology is formed as a result of phase separation between the water and the organic material upon freezing. As the ice sublimates, the organic solute concentration increases, resulting in a viscous glassy structure. This process, as demonstrated in laboratory experiments, results in a residual porous aerosol, which we termed highly porous aerosol (HPA) [*Adler et al*., 2013].

In *Adler et al*. [2013], the optical properties of HPA formed from natural organic material (NOM) were examined using cavity ring down aerosol spectroscopy (CRD-AS) [*Flores et al*., 2012; *Riziq et al*., 2007] at 0.532 μm and 0.355 μm wavelength. Significant decreases in the aerosol particle extinction efficiency of the NOM HPA, as compared to the extinction efficiency of homogeneous particles composed of the same organic material before the freezing-sublimation process, were observed for a variety of particle sizes [*Adler et al*., 2013, their Figure 4]. In *Adler et al*. [2014], a number of theoretical approaches for modeling the optical extinction of the NOM HPA were explored, including effective medium approximations (EMAs) [e.g., *Bohren and Huffman*, 1983; *Chýlek et al*., 2000; *Erlick*, 2006; *Sen et al*., 1981], extended effective

medium approximations [*Chýlek et al*., 1984; *Chýlek and Srivastava*, 1983; *Chýlek et al*., 2000; *Kolokolova and Gustafson*, 2001; *Sihvola and Sharma*, 1999; *Stroud and Pan*, 1978], multilayer concentric sphere models [e.g., *Voshchinnikov et al*., 2005; *Voshchinnikov and Mathis*, 1999; *Voshchinnikov et al*., 2007], Rayleigh-Debye-Gans theory [e.g., *Berry and Percival*, 1986; *Bonczyk and Hall*, 1991; *Sorensen*, 2001], and the discrete dipole approximation (DDA) [e.g., *Draine*, 1988, 2000; *Draine and Flatau*, 1994; *Draine and Goodman*, 1993; *Mc Donald*, 2007; *Mc Donald et al*., 2009; *Purcell and Pennypacker*, 1973; *Yurkin and Hoekstra*, 2007, 2011]. (See *Adler et al*. [2014] for a full description of these theoretical approaches and their application.) It was found that the theoretical approaches predict too much of a decrease in extinction efficiency; i.e., the theoretical approaches used in *Adler et al*. [2014] consistently underestimate the extinction by the NOM HPA as compared to the CRD-AS measurements, by up to a factor of ~2. Possible sources of error in both the calculations and the measurements were discussed thoroughly in *Adler et al*. [2014], but the source of the discrepancy was not resolved.

Note that it is rare that such theoretical calculations are compared against controlled laboratory measurements. To the best of our knowledge, in *Adler et al*. [2014], we were the first to compare theoretical calculations using the DDA against controlled laboratory measurements of extinction by particles. Some previous studies have compared theoretical calculations to ambient measurements, which are subject to additional uncertainties, including uncertainty in the exact particle size and composition, as well as subject to difficulties in modeling larger particles sizes that occur in ambient aerosol particle samples [*Adachi et al*., 2010; *Chamaillard et al*., 2006; *Lindqvist et al*., 2011, 2012; *Worringen et al*., 2008]. By comparing our theoretical calculations to controlled laboratory measurements of extinction by particles, we can better assess our level of understanding of the mechanisms controlling the optical properties of porous particles, which is fundamentally important to many disciplines, such as to aerosol science and to biomedical optics.

In the current study, we present two new sets of calculations of the extinction efficiency of HPA. The first set of calculations is a more thorough sensitivity study of the effect of void size on the calculated extinction using the DDA model ADDA [*Yurkin and Hoekstra*, 2011, 2014], with voids treated as near vacuum dielectrics. In the second set of calculations, we introduce an EMA style approach in which the voids are assigned an apparent polarizability and associated apparent indices of refraction based on the solution to Laplace's equation for a spherical cavity within a dielectric medium. (See section 2 for more detail.)

Among the conclusions we stated in *Adler et al*. [2014], it is useful to mention here that we found that the calculated extinction efficiency is not very sensitive to variations in the index of refraction of NOM within the uncertainty in the index of refraction of pure NOM that we retrieved using CRD-AS before the freezing-sublimation process, or to any roughness in the outer envelope of the (largely spherical) NOM HPA particles. By far, the calculations reported in *Adler et al*. [2014] were most sensitive to the uncertainty in the overall diameter of each HPA particle. In the current study, we retain this sensitivity to the overall diameter by conducting each calculation three times, using the mean overall diameter, using the mean overall diameter minus the uncertainty in the mean overall diameter, and using the mean overall diameter plus the uncertainty in the mean overall diameter, as measured for each HPA particle size, respectively. (See section 2 for more details.)

2. Methods

2.1. Calculations With the DDA Model ADDA

For the current study, the HPA are generated "by hand," not using a predefined shape library or the shape generation functions that are built-in to ADDA [*Yurkin and Hoekstra*, 2011, 2014]. While ADDA does offer a "granules" option, the volume fraction of such granules is limited to below the volume fractions of the voids that correspond to the porosity of our measured HPA. Furthermore, the ADDA granules option does not necessarily create the exact volume fraction desired, since it is designed to preserve the chosen size and the sphericity of the granules. To generate our "handmade" targets, first a homogeneous spherical particle of pure NOM with the diameter measured for the HPA in *Adler et al*. [2013] is generated as a collection of dipoles, and volume adjustment (as in *Yurkin and Hoekstra* [2011, their Figure 1b]) is conducted. Next voids placed at random are carved out of the previously homogeneous spherical particle of pure NOM one by one. Within each void that is being carved out, the dipoles of NOM are switched to "void dipoles" one by one, and the current overall porosity of the target is calculated; when the overall porosity of the target

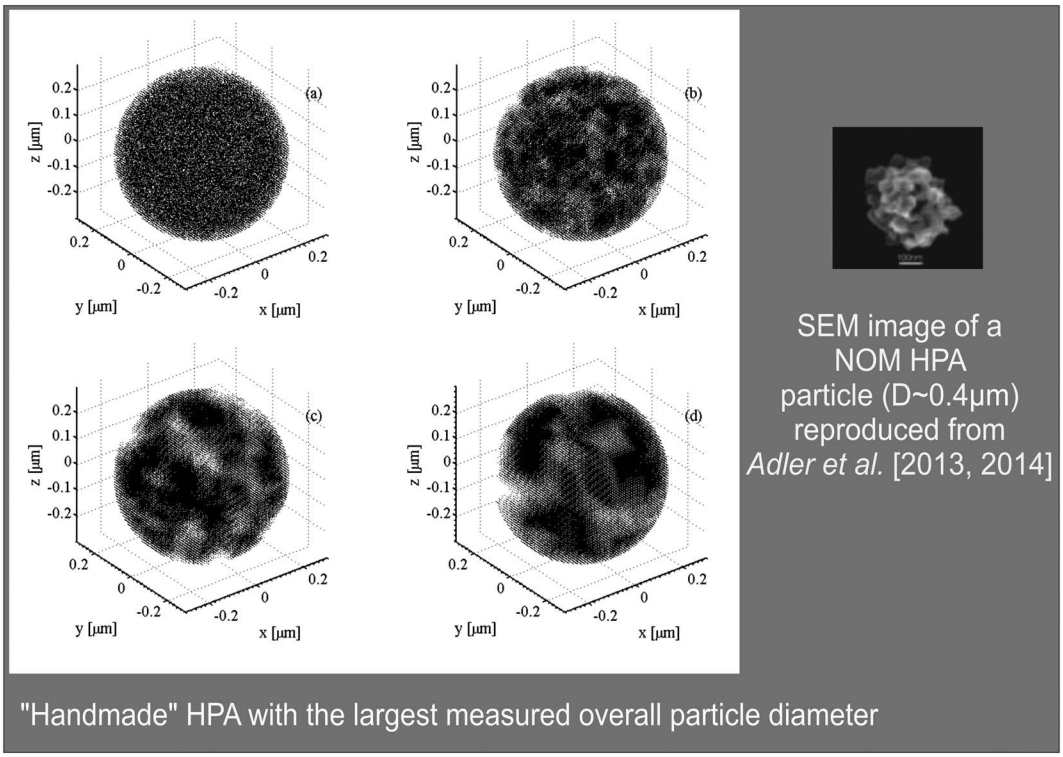

Figure 1. (left) Four realizations of a "handmade" HPA with the largest measured overall particle diameter (D_{HPA} = 0.594 μm) and with varying values of void radius: (a) void radius 0.005 μm, (b) void radius 0.03 μm, (c) void radius 0.05 μm, and (d) void radius 0.10 μm. (right) SEM image of a NOM HPA particle (~400 nm) formed following a freeze-drying cycle of a 250 nm NOM particle (reproduced from *Adler et al*. [2013, 2014]).

matches as closely as possible the measured porosity of the given HPA, the void currently being carved out is left as is (mid-void). Depending on the dipole resolution, the resulting porosity of the target is generally within 1% of the measured porosity.

The random placement of the voids is achieved by selecting three random numbers at a time, each by a call to the function rand() within the programming language C99, to calculate the position of a void in the *x*, *y*, and *z* directions, respectively. In the random placement, voids are allowed to overlap with one another, creating voids that are de facto of different sizes and shapes, even though the radius of each void that is carved out is held constant during each realization of the "handmade" target generation algorithm (see below). In addition, voids are allowed to overlap with the outer surface of the overall particle itself so that the surface is not smooth. (The part of a void overlapping with an existing void or voids does not add to the porosity; i.e., the void volume is not double counted. Likewise, if part of a void that overlaps with the outer envelope of the particle extends beyond the space of the original homogeneous particle, that part of the void is neither added to the porosity nor is it labeled a "void dipole.")

Allowing the voids to overlap with one another and with the outer surface of the particle is designed so as to replicate as closely as possible the real physical features of the HPA. As evidenced in *Adler et al*. [2013, their Figure 1], the freeze-drying process creates nonuniform voids with different sizes and shapes as well as a roughened outer surface of the particle. A number of studies have noted the effect of variations in the process of freezing on variations in void formation. For example, the porosity of spray freeze-dried materials is reported to be higher than the porosity that results from other dehydration processes [*Rahman*, 2001; *Zijlstra et al*., 2004]. Surface tension, structure, environmental pressure, and mechanisms of moisture transport also play important roles in controlling the formation of pores [*Rahman*, 2001]. In addition, pore formation is dependent on the cooling rate in the process of crystallization and crystal growth; a slower cooling rate results in a more porous structure [*Rahman*, 2001; *Schoof et al*., 2001]. In fact, the dominant void size in the particles generated in *Adler et al*. [2013] is likely to vary from overall particle size to overall particle

size; since the measurements in *Adler et al*. [2013] were conducted on a population of aerosol particles size selected and freeze-dried in a flow tube, the particles experienced different temperature ranges along the laminar flow pattern. Aside from allowing the voids to overlap, to test the sensitivity of the calculations to void size, for each of the six overall particle diameters measured in *Adler et al*. [2013, 2014] ($D_{HPA} = 0.307 \pm 0.039$, 0.354 ± 0.045, 0.412 ± 0.093, 0.479 ± 0.047, 0.515 ± 0.026, and 0.594 ± 0.040, respectively), 33 realizations of the handmade porous particle generation algorithm are used to create the corresponding target input files to ADDA, with void radii (constant over each realization, as mentioned above) of 0.005, 0.01, 0.02, 0.03, 0.04, 0.05, 0.06, 0.07, 0.08, 0.09, and 0.1 μm, respectively. (Each of the 11 void radii, respectively, are applied to the mean overall particle diameter, the mean overall particle diameter plus the uncertainty in the overall particle diameter, and the mean overall particle diameter minus the uncertainty in the overall particle diameter, respectively, for each of the six overall particle diameters, respectively.) For the purposes of visualization, four realizations of the handmade porous particle generation algorithm are shown in Figure 1 for the mean overall particle diameter of the largest HPA measured ($D_{HPA} = 0.594$ μm) and with four different selections of void radius.

For the ADDA simulations, the voids are assigned a near vacuum complex refractive index, $m_{void} = 1.0001 + i0.000$, as recommended by the program ADDA. ADDA is run on 12 processors using MPI. The formulae chosen for the scattering quantities are by *Draine* [1988], the prescription for the interaction term is as point dipoles, and the polarizability prescription is the lattice dispersion relation polarizability prescription, which includes radiation correction. The dipole resolution before volume adjustment is set at 0.01 μm. No symmetries are assumed, and using the default orientation averaging parameters of ADDA, the extinction is averaged over 226 orientations for each target.

2.2. Calculations With an EMA Style Approach With Apparent Void Polarizability

The concept of using an apparent or effective dipole moment or polarizability to describe the electromagnetic properties of a void can be found in *Rayleigh* [1897] and *Bethe* [1944] and is demonstrated in *Jackson* [1975, his sections 3.13, 5.13, and 9.5]. The basic idea as we apply it for the purposes of the current study is as follows. If a uniform, parallel external electric field of magnitude $E_{dielectric}$ is applied within a dielectric medium containing a cavity, the resulting electric field inside and outside of the cavity may be obtained by solving Laplace's equation with appropriate boundary conditions (see, e.g., *Stratton* [1941, his section 3.24], *Jackson* [1975, his section 4.4], or any textbook on classical electromagnetic theory). According to this well-known solution, the presence of the cavity creates an induced field in the dielectric medium that may be associated with a dipole moment oriented oppositely to $E_{dielectric}$ (e.g., *Stratton* [1941, his Chapter 3, Equation 32]):

$$p_{cavity} = -\frac{\varepsilon_{dielectric} - \varepsilon_{cavity}}{\varepsilon_{cavity} + 2\varepsilon_{dielectric}} 4\pi\varepsilon_{dielectric} R_{cavity}^3 E_{dielectric}, \quad (1)$$

and this is due to the fact that the walls of the cavity bear a bound charge as a result of the polarization of charge within the dielectric medium. To emphasize this well-known result, according to *Stratton* [1941, his section 3.24], "Apparently even a spherical cavity behaves like a dipole."

Equation (1) describes the dipole moment of the cavity in terms of $E_{dielectric}$. If we want to know what the value of the same dipole moment of the cavity would be relative to a uniform, parallel electric field of magnitude E_0 were it to exist in free space, we assume that any electric field within the dielectric medium would be reduced by a factor of $\frac{1}{\varepsilon_{dielectric}/\varepsilon_0}$ with respect to E_0 (see, e.g., *Jackson* [1975, p. 146]), i.e., $E_{dielectric} = \frac{\varepsilon_0}{\varepsilon_{dielectric}} E_0$, and therefore,

$$p_{cavity\ relative\ to\ free\ space} = -\frac{\varepsilon_{dielectric} - \varepsilon_{cavity}}{\varepsilon_{cavity} + 2\varepsilon_{dielectric}} 4\pi\varepsilon_0 R_{cavity}^3 E_0. \quad (2)$$

We note that equations (1) and (2) should be correct for the case of a complex permittivity of the surrounding dielectric medium as well as for the case of a purely real permittivity of the surrounding medium (e.g., *Böttcher and Bordewijk* [1996, their section 51]).

Based on the dipole moment in equation (2), we define the apparent polarizability of a void to be

$$\alpha^{\text{apparent}} = -\frac{3d^2}{4\pi}\frac{\varepsilon_{\text{dielectric}} - \varepsilon_{\text{cavity}}}{\varepsilon_{\text{cavity}} + 2\varepsilon_{\text{dielectric}}}, \tag{3}$$

where d is the diameter of the (spherical) void. Taking $\varepsilon_{\text{cavity}}$ to be the true permittivity of the void (rather than the apparent permittivity of the void; see below) and assuming that this true permittivity is the permittivity of free space (ε_0), we obtain

$$\alpha^{\text{apparent}} = -\frac{3d^2}{4\pi}\frac{\varepsilon_{\text{dielectric}} - \varepsilon_0}{\varepsilon_0 + 2\varepsilon_{\text{dielectric}}}. \tag{4}$$

Next, we equate equation (4) with the Clausius-Mossotti polarizability formula (which presents the connection between the permittivity, the size of the dipole, and the polarizability in its simplest form; e.g., *Yurkin and Hoekstra* [2011, their Equation 12]):

$$\alpha^{\text{CM}} = +\frac{3d^2}{4\pi}\frac{\varepsilon_{\text{void}}^{\text{apparent}} - \varepsilon_0}{\varepsilon_{\text{void}}^{\text{apparent}} + 2\varepsilon_0}, \tag{5}$$

and solving for $\varepsilon_{\text{void}}^{\text{apparent}}$, we obtain

$$\varepsilon_{\text{void}}^{\text{apparent}} = \frac{\varepsilon_0^2}{\varepsilon_{\text{dielectric}}}. \tag{6}$$

Using the result of equation (6), we then calculate the apparent (complex) index of refraction of the voids by taking the complex square root of $\varepsilon_{\text{void}}^{\text{apparent}}$, i.e., $m_{\text{void}}^{\text{apparent}} = \left(\frac{\varepsilon_{\text{void}}^{\text{apparent}}}{\varepsilon_0}\right)^{1/2}$ (ignoring or assuming no difference in permeability from the permeability of free space).

One should keep in mind that strictly speaking, the local (total macroscopic) electric displacement field inside of a given void comprised of pure vacuum, $\vec{D}_{\text{inside void}}$, should be equal to the permittivity of free space times the local (total macroscopic) electric field inside of the same void, $\vec{E}_{\text{inside void}}$, i.e., $\vec{D}_{\text{inside void}} = \varepsilon_0\vec{E}_{\text{inside void}}$. Defining an apparent polarizability, apparent permittivity, and apparent complex index of refraction of the voids (based on the actual dipole moment of the voids) alludes to the ability of the voids to contribute to the electric field *outside* of the voids (in the medium that surrounds them).

As mentioned above, the concept of using an apparent or effective dipole moment or polarizability to describe the electromagnetic properties of a void has been around for some time [*Rayleigh*, 1897; *Bethe*, 1944; *Jackson*, 1975, his sections 3.13, 5.13, and 9.5]. However, to the best of our knowledge, this is the first time that the concept of apparent polarizability is adopted for the purposes of calculating the extinction of electromagnetic radiation by porous dielectric particles.

The complex values of $\varepsilon_{\text{dielectric}}$ used in the current study correspond to the complex indices of refraction of the homogeneous NOM (before the freezing-sublimation) as retrieved by *Adler et al*. [2013, 2014] using CRD-AS, namely, $m_{\text{dielectric}} = 1.593 + i0.084$ at 0.532 μm wavelength and $m_{\text{dielectric}} = 1.602 + i0.136$ at 0.355 μm wavelength, where $\varepsilon_{\text{dielectric}} = \varepsilon_0\, m_{\text{dielectric}}^2$ (again ignoring or assuming no difference in permeability from the permeability of free space). Using these values of $m_{\text{dielectric}}$, the apparent indices of refraction of the voids from equation (6) come out to be $m_{\text{void}}^{\text{apparent}} = 0.626 + i(-0.0330)$ at 0.532 μm wavelength and $m_{\text{void}}^{\text{apparent}} = 0.620 + i(-0.0526)$ at 0.355 μm wavelength. (Note that these unusual values of index of refraction are apparent values only, corresponding to the apparent void polarizability, which as mentioned above has opposite sign to the polarizability of the dielectric material due to the polarization being in the opposite direction to that of the dielectric material.)

For the simulations with apparent void polarizability, the complex permittivities $\varepsilon_{\text{dielectric}}$ and $\varepsilon_{\text{void}}^{\text{apparent}}$ (or the complex indices of refraction $m_{\text{dielectric}}$ and $m_{\text{void}}^{\text{apparent}}$) at each wavelength, respectively, are combined using the Bruggeman EMA [*Bruggeman*, 1935; *Polder and Vansanten*, 1946]. The combined indices of refraction (the effective indices of refraction of each overall HPA particle) are then used as input to a homogeneous sphere Mie scattering algorithm [*Bohren and Huffman*, 1983, Appendix A] in order to calculate the extinction efficiency of each HPA.

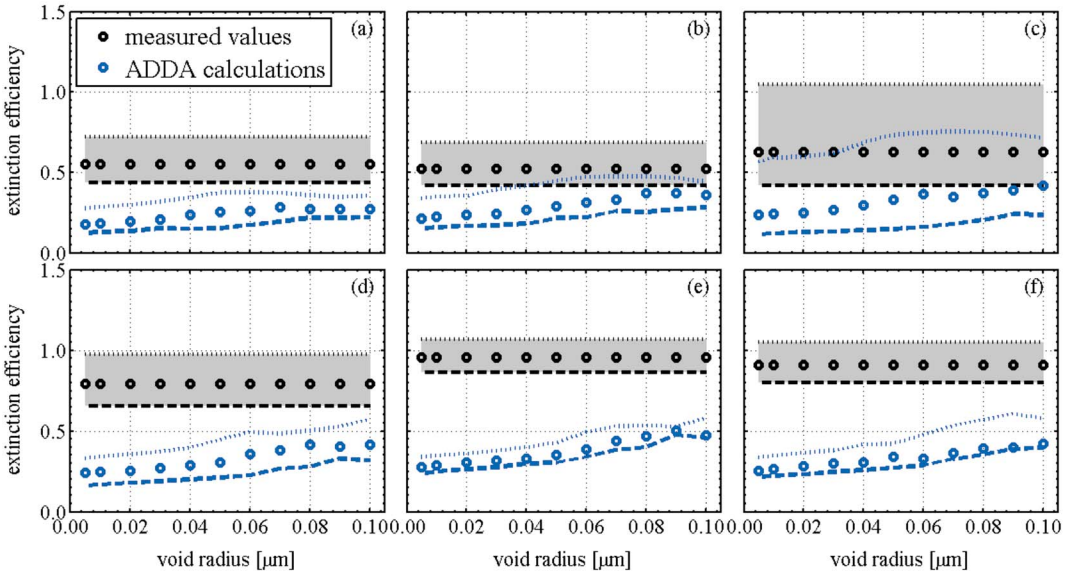

Figure 2. Extinction efficiency as a function of void radius at 0.532 μm wavelength for each of the six overall particle diameters of the HPA (D_{HPA}) measured in *Adler et al*. [2013, 2014]: (a) 0.307 ± 0.039 μm, (b) 0.354 ± 0.045 μm, (c) 0.412 ± 0.093 μm, (d) 0.479 ± 0.047 μm, (e) 0.515 ± 0.026 μm, and (f) 0.594 ± 0.040 μm. Black circles: Mean value of the measured extinction from *Adler et al*. [2013, 2014]; dashed black curve: lower bound of the measured extinction from *Adler et al*. [2013, 2014]; dotted black curve: upper bound of the measured extinction from *Adler et al*. [2013, 2014]; blue circles: calculated extinction assuming near vacuum voids, using the mean measured overall particle diameter; blue dotted line: calculated extinction assuming near vacuum voids, using the lower bound of the measured overall particle diameter; blue dashed line: calculated extinction assuming near vacuum voids, using the upper bound of the measured overall particle diameter.

2.3. Laboratory Measurements of the HPA

A full description of the setup of the measurements to which the calculations in the current study are compared can be found in *Adler et al*. [2013]. For reference, we also give a brief description here. Aerosol droplets were generated by an atomizer from a NOM standard solution (International Humic Substances Society-IHSS 1R101N). The droplets were then dried using silica gel denuders (relative humidity at the exit <3%) and size selected using a differential mobility analyzer. The size-selected aerosol particles were then humidified using a Nafion humidifier producing a relative humidity of ~ 96% ± 3%). Next, the aerosol particles were introduced into a freeze-drying reactor, which is a two-stage cooling and drying unit maintained at a temperature of 215 K via circulation of cooled ethanol. The thermodynamic path of the aerosols as they underwent freezing in the first stage of the unit and sublimated and vitrified in the second stage of the unit, as well as a full description of the system, is detailed in *Adler et al*. [2013]. The aerosol size distribution was measured using a scanning mobility particle sizer. As mentioned above, the extinction efficiency of the original homogeneous NOM aerosol particles and of the NOM HPA, respectively, was measured using a cavity ring down spectrometer at 0.532 μm and 0.355 μm wavelength, respectively.

3. Results

The calculated extinction as compared to the extinction measured in *Adler et al*. [2013, 2014] is shown in Figures 2–5, where the black symbols are used for the measured values, the blue symbols are used for the ADDA calculations with near vacuum voids, and the red symbols are used for the calculations with apparent void polarizability within the Bruggeman EMA. The results with the measurements and the ADDA calculations as a function of void radius are shown in Figures 2 and 3 for 0.532 μm and 0.355 μm wavelength, respectively. The results with the measurements, the ADDA calculations, and the calculations with apparent void polarizability, as a function of overall particle size parameter, $x \equiv \frac{\pi D_{HPA}}{\lambda}$, where λ is the wavelength, are shown in Figures 4 and 5 for 0.532 μm and 0.355 μm wavelength, respectively.

From Figures 2 and 3, several interesting features emerge. First, we find that variation in the void radius can significantly affect the calculated extinction even for the same overall particle diameter, composition, and

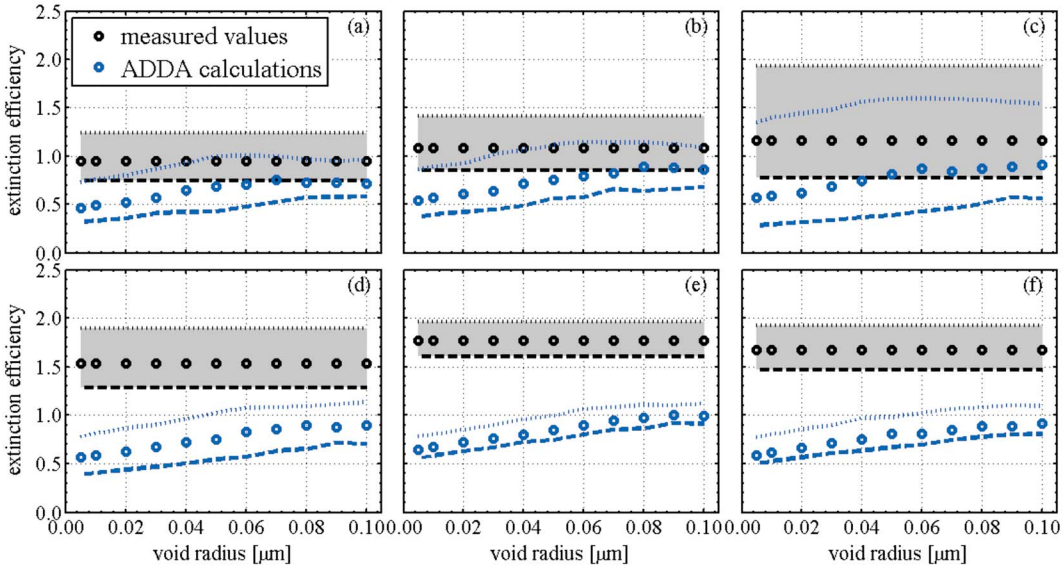

Figure 3. Extinction efficiency as a function of void radius at 0.355 μm wavelength for each of the six overall particle diameters of the HPA (D_{HPA}) measured in *Adler et al.* [2013, 2014]. Panels and symbols are the same as in Figure 2.

volume of material; we find variations of up to a factor of 2 due to void radius alone. There is a tendency for larger void radii to produce larger extinction efficiencies, but this tendency is not absolute; depending on overall particle size (and wavelength), there is in some cases at least a local maximum in efficiency at a sort of "resonant" void radius of 0.07, 0.08, or 0.09 μm. Nonetheless, uncertainty in the overall particle diameter (the difference between the dotted curves and the dashed curves) remains the primary factor affecting the range of the calculated extinction, as we concluded in *Adler et al.* [2014]. The second interesting feature of Figures 2 and 3 is that for a given HPA (for each panel in Figures 2 and 3), the calculations with smaller overall particle diameter (the dotted blue lines) exhibit the highest values of calculated extinction efficiency, whereas the calculations with larger overall particle diameter (the dashed blue lines) exhibit the lowest values of calculated extinction efficiency. This is due to the nonlinearity of the phenomenon of elastic scattering in the size regime in which the scatterer (here the overall porous particle) is of the same magnitude as the wavelength of the radiation ("the Mie scattering regime") and to the fact that with larger overall particle diameter (but with the same mass of NOM), the porosity is higher.

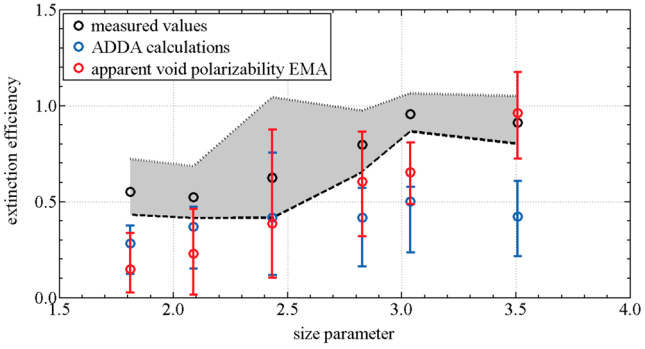

Figure 4. Extinction efficiency as a function of size parameter of the HPA ($x = \frac{\pi D_{HPA}}{\lambda}$, where D_{HPA} is the diameter of the HPA and λ is the wavelength) at 0.532 μm wavelength. Black circles: mean value of the measured extinction from *Adler et al.* [2013, 2014]; dotted black curve: upper bound of the measured extinction from *Adler et al.* [2013, 2014]; dashed black curve: lower bound of the measured extinction from *Adler et al.* [2013, 2014]; blue circles: highest value of the calculated extinction assuming near vacuum voids, using the mean measured overall particle diameter, accounting for variations in void radius; blue error bars: minimal and maximal values of the calculated extinction assuming near vacuum voids, accounting for the standard deviation of the measured overall particle diameter and accounting for variations in void radius; red circles: highest value of the calculated extinction with apparent void polarizability within the Bruggeman EMA, using the mean measured overall particle diameter, accounting for variations in void radius; red error bars: minimal and maximal values of the calculated extinction with apparent void polarizability within the Bruggeman EMA, accounting for the standard deviation of the measured overall particle diameter and accounting for variations in void radius.

From Figures 4 and 5, for the three smaller overall particle diameters, the ADDA calculations with voids with near

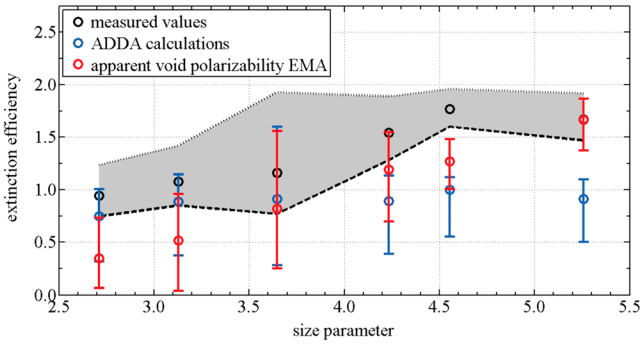

Figure 5. Extinction efficiency as a function of size parameter of the HPA at 0.355 μm wavelength. Symbols are the same as in Figure 4.

vacuum indices of refraction (blue circles with blue error bars) are satisfactory in comparison with the measured extinction (black circles and black dotted and dashed lines). (For the smallest overall particle diameter and 0.532 μm wavelength, both types of calculations underestimate the measured extinction, but the error bars of the ADDA calculations come closer to the measurements than the calculations with the apparent void polarizability EMA (red circles with red error bars).) For the three larger sizes, the calculations with the apparent void polarizability EMA fare better than the ADDA calculations; the difference is particularly noticeable for the largest HPA diameter, for which even the error bars of the ADDA calculations do not come close to the measured values nor to the error bars of the apparent void polarizability calculations. This success of the apparent void polarizability EMA for the larger HPA sizes is a logical result, since one would expect the phenomenon of apparent polarizability to be most appropriate as the size of the target grows (as the dielectric surrounding the voids becomes a large enough medium unto itself).

4. Summary and Conclusions

In summary, following our previous study, *Adler et al.* [2014], we completed two new sets of calculations of the extinction efficiency of HPA. First, we described the voids as near vacuum dielectrics within the DDA model ADDA and conducted a sensitivity study on the effect of void radius on the calculated extinction. Second, we described the voids as having an apparent polarizability based on their dipole moments within an EMA style framework. We found that when the voids are described explicitly, void size can have a significant effect on the calculated extinction, but that the uncertainty in the overall particle diameter remains a more dominant factor than void size. We found that for particles of overall diameter less than or equal to ~0.4 μm, treating the voids as near vacuum dielectrics is satisfactory in comparison to the measured extinction, with certain "resonant" void radii producing higher extinction values than others. However, for particles of overall diameter greater than ~0.4 μm, the apparent void polarizability EMA style approach produces an extinction closer to the measured extinction. We conclude that for particles of large enough overall diameter with respect to the wavelength of the radiation, apparent void polarizability is a useful concept for predicting the extinction of radiation by a porous scatterer.

Acknowledgments

The methods used in this work are detailed in the text. Data from the CRD extinction measurements are available by request from G.A. (gabriela.adler@noaa.gov). Output from the handmade target generation algorithm and extinction values output from ADDA are available by request from C.H. (caryn@vms.huji.ac.il). G.A. is an awardee of the Weizmann Institute of Science National Postdoctoral Award Program for Advancing Women in Science. The authors thank Y. Rudich for prior support and helpful suggestions and three reviewers for their helpful comments. C.H. thanks M. Haspel for suggesting the relevant section in *Stratton* [1941].

References

Adachi, K., S. H. Chung, and P. R. Buseck (2010), Shapes of soot aerosol particles and implications for their effects on climate, *J. Geophys. Res.*, *115*, D15206, doi:10.1029/2009JD012868.

Adler, G., T. Koop, C. Haspel, I. Taraniuk, T. Moise, I. Koren, R. H. Heiblum, and Y. Rudich (2013), Formation of highly porous aerosol particles by atmospheric freeze-drying in ice clouds, *Proc. Natl. Acad. Sci. U.S.A.*, *110*(51), 20,414–20,419, doi:10.1073/pnas.1317209110.

Adler, G., C. Haspel, T. Moise, and Y. Rudich (2014), Optical extinction of highly porous aerosol following atmospheric freeze drying, *J. Geophys. Res. Atmos.*, *119*, 6768–6787, doi:10.1002/2013JD021314.

Berry, M. V., and I. C. Percival (1986), Optics of fractal clusters such as smoke, *Opt. Acta*, *33*(5), 577–591.

Bethe, H. A. (1944), Theory of diffraction by small holes, *Phys. Rev.*, *66*(7/8), 163–182, doi:10.1103/PhysRev.66.163.

Bohren, C. F., and D. R. Huffman (1983), *Absorption and Scattering of Light by Small Particles*, Wiley, New York.

Bonczyk, P. A., and R. J. Hall (1991), Fractal properties of soot agglomerates, *Langmuir*, *7*(6), 1274–1280, doi:10.1021/la00054a042.

Böttcher, C. J. F., and P. Bordewijk (1996), *Theory of Electric Polarization, Volume II, Dielectrics in Time-Dependent Fields*, 2nd ed., Elsevier, Amsterdam.

Bruggeman, D. A. G. (1935), Berechnung verschiedener physikalischer Konstanten von heterogenen Substanzen. I. Dielektrizitätskonstanten und Leitfähigkeiten der Mischkörper aus isotropen Substanzen, *Ann. Phys.*, *416*(7).

Chamaillard, K., C. Kleefeld, S. G. Jennings, D. Ceburnis, and C. D. O'Dowd (2006), Light scattering properties of sea-salt aerosol particles inferred from modeling studies and ground-based measurements, *J. Quant. Spectrosc. Radiat. Transfer*, *101*(3), 498–511, doi:10.1016/j.jqsrt.2006.02.062.

Chýlek, P., and V. Srivastava (1983), Dielectric-constant of a composite inhomogeneous-medium, *Phys. Rev. B*, *27*(8), 5098–5106, doi:10.1103/PhysRevB.27.5098.

Chýlek, P., V. Ramaswamy, and R. J. Cheng (1984), Effect of graphitic carbon on the albedo of clouds, *J. Atmos. Sci.*, *41*(21), 3076–3084, doi:10.1175/1520-0469(1984)041.

Chýlek, P., G. Videen, D. J. W. Geldart, J. S. Dobbie, and H. C. W. Tso (2000), Effective medium approximations for heterogeneous particles, in *Light Scattering by Nonspherical Particles, Theory, Measurements, and Applications*, Academic Press, New York.

Draine, B. T. (1988), The discrete-dipole approximation and its application to interstellar graphite grains, *Astrophys. J.*, *333*(2), 848–872, doi:10.1086/166795.

Draine, B. T. (2000), The discrete dipole approximation for light scattering by irregular targets, in *Light Scattering by Nonspherical Particles: Theory, Measurements, and Applications*, Academic Press, New York.

Draine, B. T., and J. Goodman (1993), Beyond Clausius-Mossotti—Wave-propagation on a polarizable point lattice and the discrete dipole approximation, *Astrophys. J.*, *405*(2), 685–697, doi:10.1086/172396.

Draine, B. T., and P. J. Flatau (1994), Discrete-dipole approximation for scattering calculations, *J. Opt. Soc. Am. A*, *11*(4), 1491–1499, doi:10.1364/Josaa.11.001491.

Erlick, C. (2006), Effective refractive indices of water and sulfate drops containing absorbing inclusions, *J. Atmos. Sci.*, *63*(2), 754–763, doi:10.1175/Jas3635.1.

Flores, J. M., R. Z. Bar-Or, N. Bluvshtein, A. Abo-Riziq, A. Kostinski, S. Borrmann, I. Koren, I. Koren, and Y. Rudich (2012), Absorbing aerosols at high relative humidity: Linking hygroscopic growth to optical properties, *Atmos. Chem. Phys.*, *12*(12), 5511–5521, doi:10.5194/acp-12-5511-2012.

Jackson, J. D. (1975), *Classical Electrodynamics*, 2nd ed., John Wiley, New York.

Jeong, G. Y., and T. Nousiainen (2014), TEM analysis of the internal structures and mineralogy of Asian dust particles and the implications for optical modeling, *Atmos. Chem. Phys.*, *14*(14), 7233–7254, doi:10.5194/acp-14-7233-2014.

Kolokolova, L., and B. A. S. Gustafson (2001), Scattering by inhomogeneous particles: Microwave analog experiments and comparison to effective medium theories, *J. Quant. Spectrosc. Radiat. Transfer*, *70*(4-6), 611–625, doi:10.1016/S0022-4073(01)00033-4.

Kylling, A., M. Kahnert, H. Lindqvist, and T. Nousiainen (2014), Volcanic ash infrared signature: Porous non-spherical ash particle shapes compared to homogeneous spherical ash particles, *Atmos. Meas. Tech.*, *7*(4), 919–929, doi:10.5194/amt-7-919-2014.

Lindqvist, H., T. Nousiainen, E. Zubko, and O. Munoz (2011), Optical modeling of vesicular volcanic ash particles, *J. Quant. Spectrosc. Radiat. Transfer*, *112*(11), 1871–1880, doi:10.1016/j.jqsrt.2011.01.032.

Lindqvist, H., T. Nousiainen, E. Zubko, and O. Munoz (2012), Optical modeling of vesicular volcanic ash particles, *J. Quant. Spectrosc. Radiat. Transfer*, *113*(2), 199–199, doi:10.1016/j.jqsrt.2011.09.014.

Mc Donald, J. (2007), *Open DDA – A Novel High-Performance Computational Framework for the Discrete Dipole Approximation*, National Univ. of Ireland, Galway.

Mc Donald, J., A. Golden, and S. G. Jennings (2009), OpenDDA: A novel high-performance computational framework for the discrete dipole approximation, *Int. J. High Perform. Comput. Appl.*, *23*, 42–61.

Polder, D., and J. H. Vansanten (1946), The effective permeability of mixtures of solids, *Physica*, *12*(5), 257–271, doi:10.1016/S0031-8914(46)80066-1.

Purcell, E. M., and C. R. Pennypacker (1973), Scattering and absorption of light by nonspherical dielectric grains, *Astrophys. J.*, *186*(2), 705–714, doi:10.1086/152538.

Rahman, M. S. (2001), Toward prediction of porosity in foods during drying: A brief review, *Dry Technol.*, *19*(1), 1–13, doi:10.1081/Drt-100001349.

Rayleigh, L. (1897), On the incidence of aerial and electric waves upon small obstacles in the form of ellipsoids or elliptic cylinders and on the passage of electric waves through a circular aperture in a conducting screen, *Philos. Mag.*, *44*, 28–52.

Riziq, A. A., C. Erlick, E. Dinar, and Y. Rudich (2007), Optical properties of absorbing and non-absorbing aerosols retrieved by cavity ring down (CRD) spectroscopy, *Atmos. Chem. Phys.*, *7*(6), 1523–1536.

Schoof, H., J. Apel, I. Heschel, and G. Rau (2001), Control of pore structure and size in freeze-dried collagen sponges, *J. Biomed. Mater. Res.*, *58*(4), 352–357, doi:10.1002/jbm.1028.

Sen, P. N., C. Scala, and M. H. Cohen (1981), A self-similar model for sedimentary-rocks with application to the dielectric-constant of fused glass-beads, *Geophysics*, *46*(5), 781–795, doi:10.1190/1.1441215.

Sihvola, A., and R. Sharma (1999), Scattering corrections for Maxwell Garnett mixing rule, *Microwave Opt. Technol. Lett.*, *22*(4), 229–231, doi:10.1002/(Sici)1098-2760(19990820)22:4<229::Aid-Mop3>3.0.Co;2-9.

Sorensen, C. M. (2001), Light scattering by fractal aggregates: A review, *Aerosol Sci. Technol.*, *35*(2), 648–687, doi:10.1080/02786820117868.

Stratton, J. A. (1941), *Electromagnetic Theory*, McGraw-Hill, New York.

Stroud, D., and F. P. Pan (1978), Self-consistent approach to electromagnetic-wave propagation in composite media—Application to model granular metals, *Phys. Rev. B*, *17*(4), 1602–1610, doi:10.1103/PhysRevB.17.1602.

Voshchinnikov, N. V., and J. S. Mathis (1999), Calculating cross sections of composite interstellar grains, *Astrophys. J.*, *526*(1), 257–264, doi:10.1086/307997.

Voshchinnikov, N. V., V. B. Il'in, and T. Henning (2005), Modelling the optical properties of composite and porous interstellar grains, *Astron. Astrophys.*, *429*(2), 371–381, doi:10.1051/0004-6361:200400081.

Voshchinnikov, N. V., G. Videen, and T. Henning (2007), Effective medium theories for irregular fluffy structures: Aggregation of small particles, *Appl. Opt.*, *46*(19), 4065–4072, doi:10.1364/Ao.46.004065.

Wolff, M. J., G. C. Clayton, and S. J. Gibson (1998), Modeling composite and fluffy grains. II. Porosity and phase functions, *Astrophys. J.*, *503*(2), 815–830, doi:10.1086/306029.

Worringen, A., M. Ebert, T. Trautmann, S. Weinbruch, and G. Helas (2008), Optical properties of internally mixed ammonium sulfate and soot particles—a study of individual aerosol particles and ambient aerosol populations, *Appl. Opt.*, *47*(21), 3835–3845, doi:10.1364/Ao.47.003835.

Yurkin, M. A., and A. G. Hoekstra (2007), The discrete dipole approximation: An overview and recent developments, *J. Quant. Spectrosc. Radiat. Transfer*, *106*(1-3), 558–589, doi:10.1016/j.jqsrt.2007.01.034.

Yurkin, M. A., and A. G. Hoekstra (2011), The discrete-dipole-approximation code ADDA: Capabilities and known limitations, *J. Quant. Spectrosc. Radiat. Transfer*, *112*(13), 2234–2247, doi:10.1016/j.jqsrt.2011.01.031.

Yurkin, M. A., and A. G. Hoekstra (2014), User Manual for the Discrete Dipole Approximation Code ADDA 1.3b4. [Available at http://a-dda.googlecode.com/svn/tags/rel_1.3b4/doc/manual.pdf.]

Zijlstra, G. S., W. L. J. Hinrichs, A. H. de Boer, and H. W. Frijlink (2004), The role of particle engineering in relation to formulation and de-agglomeration principle in the development of a dry powder formulation for inhalation of cetrorelix, *Eur. J. Pharm. Sci.*, *23*(2), 139–149, doi:10.1016/j.ejps.2004.06.005.